Article

Performance Assessment of PPP Surveys with Open Source Software Using the GNSS GPS–GLONASS–Galileo Constellations

Antonio Angrisano [1], Gino Dardanelli [2,*], Anna Innac [3], Alessandro Pisciotta [2], Claudia Pipitone [2] and Salvatore Gaglione [3]

1   University of Benevento Giustino Fortunato, Via R. Delcogliano, 82100 Benevento, Italy; a.angrisano@unifortunato.eu
2   Department of Engineering, University of Palermo, Viale delle Scienze, 90128 Palermo, Italy; alessandro.pisciotta@community.unipa.it (A.P.); claudia.pipitone02@unipa.it (C.P.)
3   Department of Sciences and Technologies, University of Naples Parthenope, Via Ammiraglio F. Acton, 80133 Naples, Italy; anna.innac@uniparthenope.it (A.I.); salvatore.gaglione@uniparthenope.it (S.G.)
*   Correspondence: gino.dardanelli@unipa.it; Tel.: +39-091-2389-6228

Featured Application: Environmental monitoring of risk areas, deformation control of structures (dams, bridges), topographical surveying, GCP for aerial mapping survey.

Abstract: In this work, the performance of the multi-GNSS (Global Navigation Satellite System) Precise Point Positioning (PPP) technique, in static mode, is analyzed. Specifically, GPS (Global Positioning System), GLONASS, and Galileo systems are considered, and quantifying the Galileo contribution is one of the main objectives. The open source software RTKLib is adopted to process the data, with precise satellite orbits and clocks from CNES (Centre National d'Etudes Spatiales) and CLS (Collecte Localisation Satellites) analysis centers for International GNSS Service (IGS). The Iono-free model is used to correct ionospheric errors, the GOT-4.7 model is used to correct tidal effects, and Differential Code Biases (DCB) are taken from the Deutsche Forschungsanstalt für Luftund Raumfahrt (DLR) center. Two different tropospheric models are tested: Saastamoinen and Estimate ZTD (Zenith Troposhperic Delay). For the proposed study, a dataset of 31 days from a permanent GNSS station, placed in Palermo (Italy), and a dataset of 10 days from a static geodetic receiver, placed nearby the station, have been collected and processed by the most used open source software in the geomatic community. The considered GNSS configurations are seven: GPS only, GLONASS only, Galileo only, GPS+GLONASS, GPS+Galileo, GLONASS+Galileo, and GPS+GLONASS+Galileo. The results show significant performance improvement of the GNSS combinations with respect to single GNSS cases.

Keywords: GNSS; GPS; GLONASS; Galileo; PPP; RTKLib; ZTD

1. Introduction

Nowadays, Precise Point Positioning (PPP) is increasingly becoming widespread as an absolute positioning technique introducing a large variety of possible applications in both kinematic and static conditions. High-accuracy navigation and/or positioning can be performed worldwide in an absolute coordinate reference frame, and other PPP applications include the monitoring of areas subject to environmental risk, deformation controls of large structures (landslides, dams), plate tectonics studies [1,2], the determination of Ground Control Point (GCP), resource management in remote areas, and sea-level measurement [3–6]. Unlike the classical absolute positioning methods that use code measurements and the broadcast ephemeris to obtain the position of the receiver, PPP has the

advantage of using the most precise carrier phase observables, and reducing the effect of all the types of errors and biases that affect GNSS (Global Navigation Satellite System) measurements. In this way, PPP is able to provide a precision level comparable to differential positioning without the support of ground stations. For this reason, PPP is particularly suitable for remote areas.

GNSS technology is constantly changing, offering new opportunities to many applications in navigation, land surveying, and general geo-referencing. In particular, recent developments related to Europe's core constellation, Galileo, and China's own core constellation, the BeiDou navigation satellite system (BDS), have been underway and are fast oncoming completion. The introduction of these two advanced systems allows for the number of globally available GNSS satellites to be greatly grown, consequently also enhancing the robustness of GNSS as a whole.

In the last two decades, the scientific community has paid particular attention to the multi-constellation approach in PPP techniques. Since 2009, the first real-time service providing GLONASS precise orbits and clocks was available [7,8]. The use of multi-constellation double-frequency GNSS has demonstrated improved performance, in terms of precision and convergence time, with respect to single GNSS case [9,10].

In [11], the authors proposed a multi-GNSS PPP model using data from the MGEX (Multi-GNSS Experiment) and BETN (BeiDou Experimental Tracking Network) ground tracking networks to fully take advantage of all available GNSS observables. The results showed that the integration of BeiDou, Galileo and GLONASS systems with GPS (Global Positioning System) significantly shortened the convergence time and improved the positioning accuracy. In particular, for the GPS-only solution, the positioning accuracy reached the decimeter level after a convergence time of thirty minutes, and the centimeter level after about 2 h for all three components of the position. GLONASS-only PPP configuration showed a slightly worse positioning accuracy and a longer convergence compared to GPS-only PPP. The BeiDou-only PPP provided good performance on the horizontal components, achieving few centimeter accuracies within one hour. Finally, the multi-GNSS (GPS/BeiDou/GLONASS/Galileo) PPP configuration presented the fastest convergence and highest accuracy for all three components.

In 2015, the authors in [12] proposed a dual-frequency (DF) PPP model based on GPS and Galileo observables. The proposed model was based on a GPS/Galileo ionosphere-free (IF) linear combination PPP model, accounting for the additional combined biases, that are the Galileo satellite hardware delay and GPS to Galileo time offset (GGTO). These biases were lumped and considered as a new unknown parameter (noted as inter-system bias) into the PPP model. To obtain the best estimates for unknown parameters, a sequential least-squares estimation method was used. It is shown that, compared to the GPS-only configuration, 25% convergence time improvement and a sub-decimeter positioning accuracy level were achieved thanks to the developed PPP model. In 2016, the authors in [13] introduced a new DF-PPP model, combining the measurements from the GPS, Galileo, and BeiDou systems. The proposed model applies the un-differenced and between-satellite single-difference (BSSD) linear combinations. The latter is able to cancel out some biases related to the receiver, such as the non-zero initial phase bias of the receiver oscillator and receiver clock error. The statistical results showed that the post-processed GNSS PPP technique based on un-differenced observations provided a convergence time improvement of 25% with respect to the GPS-only configuration. In addition, the use of the BSSD technique in post-processing PPP mode improved the precision of the positioning solution by about 25% compared to the GPS-only case. The convergence time of the solution was equal to 10 min when the BSSD model was applied.

In [14], the benefits of multi-GNSS for PPP were also investigated. Firstly, a consistency test of precise orbit and clock products supplied by different providers (CNES, Center for Orbit Determination in Europe—CODE-, German Research Centre for Geosciences—GFZ-, etc.) were performed for GPS, GLONASS, Galileo, and BeiDou. Furthermore, to investigate the effectiveness of multi-GNSS data and higher rate precise orbit and clock products, five Asia–Pacific regional stations of the MGEX network were chosen for kinematic PPP tests adopting TriP software developed by Wuhan University [15]

and based on IF combination of DF carrier phases and pseudoranges. Furthermore, in this case, the positioning accuracy and fast convergence time benefited from the combined using of multi-GNSS and a higher rate of precise clock corrections. The multi-GNSS PPP approach improved the positioning accuracy by 20% and 80% considering the GPS-GLONASS and BeiDou-only PPP configurations. Using higher rate precise clock products allows for the effect of the errors related to the interpolation to decrease, and the positioning accuracy was enhanced by an average of 30%–50% for the all the configurations excepting for the BeiDou-only PPP.

A performance analysis of a multi-GNSS PPP model based on GPS, GLONASS, Galileo, and BeiDou observations, was also shown in [16]. The investigation on PPP accuracy and convergence time was conducted on the basis of data processing results from both kinematic and static modes considering single-and multi-constellation configurations. Data from five stations on sixteen consecutive days were used and all stations were equipped with multi-GNSS receivers. DF observations from GPS L1/L2, GLONASS G1/G2, BeiDou B1/B2, and Galileo E1/E5a signals were adopted to form the IF combined code and carrier-phase measurements model. Multi-GNSS precise satellite orbit and clock products provided by the ESOC (European Space Operations Center, Germany) were adopted for PPP techniques together with different error correction models. The results of static positioning indicated that the BeiDou-only PPP positioning accuracy was lower than the GPS-only case on both horizontal and vertical components. GPS/BeiDou PPP configuration provides a positioning accuracy improvement of 28%, 6%, and 7% in the three coordinates, respectively, with respect to the GPS-only PPP while a slightly worse positioning accuracy is achieved with GPS/GLONASS PPP. The usage of a triple-constellation GPS/BeiDou/GLONASS PPP improved the positioning accuracy by 25%, 20%, and 19% over the GPS/BeiDou and 9%, 8%, and 10% with respect to GPS/GLONASS in the east, north, and up directions. Additionally, the BeiDou-only PPP converged more slowly compared to the GPS-only PPP, but the integration of GPS and BeiDou allowed one to reduce the convergence time by 26%, 13%, and 14% in the three coordinates, respectively, over the GPS-only case. A convergence time improvement of 50%, 29%, and 33% is obtained using GPS/GLONASS PPP when compared to the GPS-only case. Finally, a larger reduction of the convergence time is obtained using triple-constellation in the PPP model. Furthermore, for the multi-constellation kinematic PPP approach, an improvement of the positioning accuracy and convergence time was highlighted compared to the single-constellation and dual-constellations cases.

In [17] the authors investigated the effectiveness of integrating GPS and GLONASS measures to improve the reliability and accuracy of positioning results using PPP. The authors showed that the integration of GLONASS satellites significantly improved the satellite availability (more than 60%) leading to the enhancement of satellite geometry (in terms of Positional Dilution of Precision—PDOP) by more than 30%. In this way, the performance of precise surveying can be improved in scenarios such as urban areas, dense vegetation, mountains areas, or when the satellite signal is partially obstructed as confirmed also in [18].

A performance analysis of multi-GNSS PPP has been conducted in [19] using DF observations from GPS, GLONASS, Galileo, BeiDou and QZSS systems. Precise multi-GNSS orbit and satellite clock products from GFZ were chosen for six stations selecting data from 150 to 160 days of 2016. If observations were used to eliminate the ionosphere delays. The receiver clock error was computed as an unknown parameter using the least square estimator. Troposphere delay was considered as a random-walk process. Furthermore, the Kalman filter was used to filter and smooth time-dependent parameters. The analysis of the results showed a positioning accuracy improvement at a centimeter level obtained thanks to the multi-GNSS configuration compared to GPS-only. However, it was highlighted that when positioning errors reach a very low level (about 5 mm) the multi-GNSS contribution is rather limited, due to the accuracy of orbit and satellite clock products of the other GNSSs as BeiDou, GLONASS, and Galileo. On the other hand, a significant increasing of the satellite availability was detected when the multi-GNSS approach was considered. Therefore, the same authors suggest that an improvement, both in terms of reliability and availability of positioning results, would be more evident

in difficult environments, such as urban areas or partially obstructed places. This same conclusion, also related to the multipath effect, was recently made by other researchers who examined the quad-GNSS PPP performance (GPS, Galileo, GLONASS, BeiDou) [20]. However, from their tests, they found a substantial performance enhancement for the GPS+GLONASS combination with respect to GPS-only.

Benefits of multi-GNSS have also been highlighted in [21], in which PPP models were performed using both single and dual frequency measurements from GPS, GLONASS, Galileo, and BeiDou systems and considering three selected stations located in Egypt at different latitudes. The IGS-MGEX final precise products were chosen for the correction of orbital and clock errors, while the final IGS GIMs (Global Ionosphere Maps) were adopted to reduce the effect of the ionospheric delay in the single-frequency (SF) PPP model. For both DF- and SF-PPP models, the results showed that the convergence time for the multi-GNSS configuration was enhanced by 35% with respect to GPS only PPP. It was also highlighted that the positioning accuracy improvement of multi-GNSS PPP is mainly due to the contribution of GLONASS observables, while the contribution of Galileo and Beidou was minimal due to their limited satellite availability.

In 2019, an evaluation of availability and performance of PPP positioning with four constellations, GPS, GLONASS, BeiDou, and Galileo, was carried out in [22]. In detail, the performance of quad-constellation DF-PPP, SF-PPP, and SPP are verified using the datasets from 59 globally distributed stations spanning 30 days. Furthermore, in this research, the results have indicated that both the availability and accuracy of positioning solutions were significantly enhanced by integrating multi-constellation signals.

As it can be noted by the literature, even if PPP usually uses DF GNSS observations, different authors propose the development of the SF-PPP model to be adopted when low-cost SF GNSS receivers are used [23–25]. On the other hand, the development of four GNSS constellations is showed also in [26].

In [27], different PPP models were developed using SF measurements from GPS, GLONASS, BeiDou, and Galileo; the un-differenced SF GNSS PPP model, the un-differenced IF code, and the carrier phase model; and the Between-Satellite-Single-Difference model (BSSD) and the Between-Satellite-Single-Difference IF (BSSDIF) models. For both un-differenced and BSSD models, the IGS final GIM model was used to correct the ionospheric delay, while the IGS final precise products were used in all the considered PPP models. Furthermore, in this work, it was highlighted that the benefit of the additional GLONASS and BeiDou observations is significant. It was also shown that the positioning accuracy obtained using IF-PPP model was significantly better than the GIM-based PPP. After 2 h of data processing, the 3D positioning accuracy was enhanced by 13 cm when the IF-PPP was used with respect to the GIM-based technique. Furthermore, comparable results were obtained from both the GPS/Galileo and GPS/BeiDou combinations. For the GPS/GLONASS configuration, the mean value of 3D positioning solutions was enhanced by 6 cm using IF-PPP technique with respect to the GIM-based model.

The aim of current study is to assess the performance of PPP positioning, using multi-frequency and multi-constellation GNSS. In detail, the adopted GNSS systems are GPS, GLONASS, and Galileo, and particularly interesting is the contribution of the latter. The considered GNSS configurations are GPS only, GLONASS only, Galileo only, GPS+GLONASS, GPS+GLONASS, GPS+Galileo, GLONASS+Galileo, and GPS+GLONASS+Galileo. Large sets of data, collected in southern Italy (Sicily), are processed in order to study the PPP performance: 31 days from a permanent station and 10 days from a static receiver placed on a pillar. Conversely to the literature, in which mainly customized PPP software are used, in the current research, the datasets are processed with the open source software RTKLib and different tropospheric models are considered: Saastamoinen and Estimate ZTD (Zenith Troposhperic Delay). The use of an open source software has the main objective of guarantying the repeatability of the experiment for scientific community interested in precise survey applications; in addition, the large amount of processed data allows one to provide significant information about the performance of the multi-GNSS PPP.

The paper is organized as follows. In Section 2, the experiment is described, providing details about the equipment and the location, and RTKLib software and its working are explained. In Section 3, the results, obtained with the considered configurations, are shown and clarified. In Section 4, the conclusions of the work are exposed.

2. Materials and Methods

2.1. Experiment: Datasets and Location

To evaluate the performance of the adopted PPP approach, two static tests are carried out, consisting of a dataset collected by a permanent station, located at Palermo University (Test A) and a dataset collected by a geodetic receiver placed nearby the station (Test B). The geographical positions of the tests are shown in Figure 1.

(**a**)   (**b**)
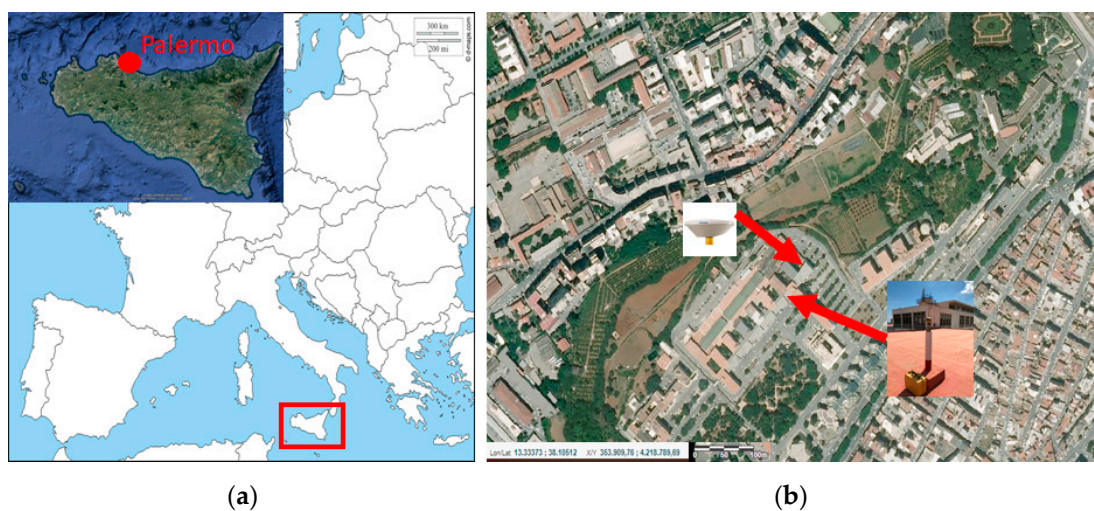
Figure 1. (**a**) Geographical position of the study area; (**b**) digital orthophoto from Italian National Geoportal, scale 1:4000, reference system UTM-WGS8433N (ETRF2000); position of Trimble permanent station and Topcon HiPer HR on a concrete pillar.

Up to 2008, in Sicily there was not a local GNSS network; thus, the University of Palermo has designed and realized the first local level-based network in the central-western part of the island. The management of the GNSS Continuously Operating Reference Station (CORS) network, consisting of 8 stations used for technical and scientific purposes, was preliminary entrusted to the University (until 2013); later, the stations were included in the Netgeo GNSS network, managed by Topcon Italy, due to the scientific collaboration between the latter and the University of Palermo, aimed to realize the first local level based network in Sicily [28]. Furthermore, two additional permanent stations are located at Palermo University: one is equipped with a Trimble NetR9 receiver and Zephyr GNSS Geodetic II antenna (belonging to Trimble RTX network) and another station of the network is managed by Hexagon Geosystems, Italian Positioning Service (ItalPoS) (HxGN SmartNet 2020), with a LEICA GMX902GG receiver and LEIAS10 NONE antenna.

The CORS network set up in the western part of Sicily has been tested and data are used for several scientific works focused on: use of Mobile Mapping System (MMS) for integrated survey [29,30], GNSS techniques for land and structure as dams monitoring [31–33], geological analyses [34], integrated survey in archaeological context [35,36], and recently also geodynamic research [37].

Test A is performed collecting data by the permanent station Trimble NetR9 located at Palermo University and considering a time interval of 31 days, starting 1 July 2018-DOY (Day of Year) 182 to 31 July 2018-DOY 212.

The considered station is equipped with the antenna TRM55971.00 TZGD (Zephyr GNSS Geodetic II) able to acquire GPS, Galileo, GLONASS, and Beidou signals. The antenna is robust and recommended for GNSS geodetic survey. The quality and precision features characterizing the antenna are the repeatability of the sub-millimeter phase center, the robust satellite tracking at low altitude, and the reduced multipath effect. The permanent station records satellite data continuously, returning daily observation and navigation files. In particular, daily data are considered, in both RINEX hatanaka 2.11 formats, consisting of the observation files (.O) and the GPS (.N), GLONASS (.G), and Galileo (.L) ephemeris files, and RINEX hatanaka 3.00 formats, consisting of the observation files (.O) and a single ephemeris file containing all the constellations analyzed (.P).

Test B is carried out using a geodetic receiver and collecting data for 10 days, starting from 18th (DOY 199) to 31st of July 2018 (DOY 212), with an acquisition session of six hours a day. The used receiver is the Topcon HiPer HR, installed daily on a pillar placed on rooftop of Palermo University. The receiver is capable of acquiring signals from GPS, GLONASS, Galileo, BeiDou, QZSS, SBAS, and L-Band in 452 channels and using Universal Tracking Channel technology. Using the described receiver, a single file is obtained in "*.tps" format. In post-processing, a dedicated converter tool of Topcon (TPS2RIN) is used to convert the file "* .tps" in two files in RINEX 3.02 format: the observation and navigation files.

In Test B, the PPP performance using a geodetic receiver with integrated antenna are evaluated. In fact, despite both used receivers (Trimble NetR9 and Topcon Hiper HR) acquiring data from GPS, GLONASS, and Galileo constellations, their antennas are different. The CORS in Palermo is equipped with a Zephyr GNSS Geodetic II antenna (TRM55971.00 TZGD), also used in the IGS (International GNSS Service) network and calibrated by NGS (National Geodetic Survey), while the Topcon receiver is an integrated antenna (micro centered Fence Antenna™ with Ground Plane) [38,39].

2.2. RTKLib Software

To perform the PPP-static technique, RTKLib version 2.4.2 p13 software is used for the data processing [40]. RTKLib is an open source positioning software developed by Dr. T.Takatsu. All the data and corrections are entered as inputs using the software Graphic User Interface. It supports standard and precise positioning algorithms with GPS, GLONASS, Galileo, QZSS, BeiDou, and SBAS. Different positioning modes are allowed using GNSS data for both real-time and post-processing such as single point positioning (absolute technique), DGNSS (differential code approach) Kinematic, Static, Moving-Baseline, Fixed (carrier-phases-based relative approach), PPP-Kinematic, PPP-Static, and PPP-Fixed.

The software consists of a program library and a series of executable files that use this library. It is possible to use the RTKLib package through the graphical interface, or the "main program" called RTKLAUNCH (Figure 2) or by running the individual CUI (command-line user interface) APs (application programs).
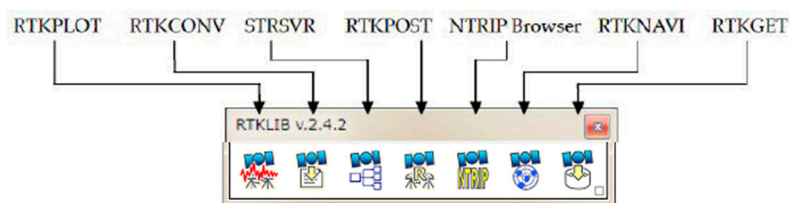

Figure 2. Screenshot of graphical user interface of the RTKLAUNCH module.

The aim of the work is to evaluate the performance of a PPP-static positioning mode, a method mainly used for scientific purposes, taking into account the incidence of the various biases, the various error correction products and the contribution of the available satellite constellations. Although the

main problem of this method is related to the long convergence time of the solutions, with a multi-GNSS integration it is possible to reduce time and also improve positioning accuracy [3,41,42].

For static PPP processing, the RTKPOST is used, which is the RTKLib module for the post processing of GNSS data. RTKPOST requires, as input, the RINEX files (containing the observations, the navigation data and also the precise orbit products if available) and returns, as output, the ".pos" format file (Figure 3). In addition to the positioning solution, the output file also provides the number of satellites used for the solution computation, the type of solution obtained, and the standard deviations estimates. In the output files, the solutions can optionally be expressed in different formats: the geographic coordinates (lat, lon, h), the Cartesian geocentric coordinates (X, Y, Z), baseline (E, N, h), and the message NMEA0183 (Figure 4).

Figure 3. Example of obtained solution extract with the RTKPOST module.
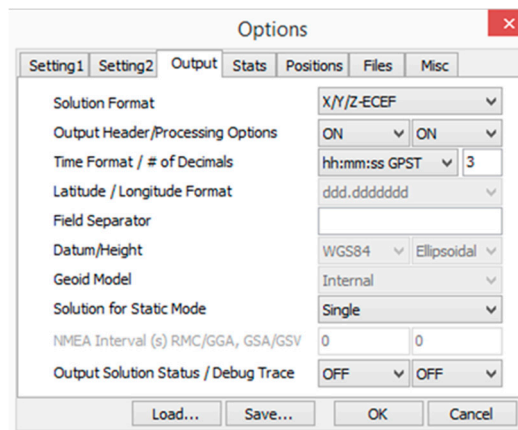
Figure 4. Output options interface with the RTKPOST module.

Based on the adopted positioning mode, RTKPOST allows one to select different settings such as the carrier frequencies (L1, L1 + L2, L1 + L2 + L5), filter type (Forward, Backward, Combined), elevation and SNR (signal noise ratio) masks, the navigation satellite systems, and several errors correction models (i.e., Earth Tides, ionosphere, troposphere) to be applied. In addition, as it is previously described, to process the observation data collected by a receiver in PPP mode using RTKPOST, several correction models must be applied selecting specified settings such as precise satellite ephemeris and clock corrections, satellite and receiver antenna phase center variations (PCV), corrections of the

tropospheric and ionospheric effects, SBAS corrections, solid earth tides, ocean tide loading, and pole tides can be also modeled.

To verify the performance improvements for PPP-static mode obtained thanks to multi-GNSS, focusing the attention on Galileo, precise satellite products for GPS, GLONASS, and Galileo are downloaded by MGEX [43]. In particular, precise products computed by CNES/CLS are selected in the current analysis. This choice is also related to the aim of testing the PPP-AR (Ambiguity Resolution) function for the resolution of the phase ambiguity that can be selected in RTKLib software. However, the results obtained applying the PPP-AR method in RTKLib have highlighted that the considered ambiguity resolution technique provides unstable and inaccurate solution with respect to standard PPP. Indeed, the tested PPP-AR processing mode is considered "experimental" in the RTKLib manual. For this reason, the results will not show in the current research.

The CNES/CLS center provides ephemeris at 15-minute intervals with clock corrections every 5 min (in ".sp3" format) and also clock corrections every 30 s (in ".clk" format). The combined use of ".sp3" and ".clk" products is useful both for real-time applications and for fixing ambiguity.

In RTKPOST different ionospheric error correction models can be chosen, including using ionospheric parameters broadcast in the navigation message, iono-free linear combination (possible only if observation data on both L1 and L2 frequencies are available and no triple frequency combinations are allowed) named Iono-Free LC, using the estimated ionospheric parameters STEC (Slant Total Electron Content), or IONEX TEC data. In the current analysis, Iono-Free LC is used as an ionospheric correction model in the IF combination of DF carrier phases and pseudoranges used in the adopted PPP measurement model. It is well known that the Iono-Free LC is able to eliminate errors of about 99.9% of ionospheric delay as shown by several studies [12,14,20], highlighting the achievement of satisfactory positioning results.

Since the test is carried out in Palermo, located about 1 km from the coast, and since high precision values are desired, the effects due to the tide are also included in the processing. Many models have been developed to correct this effect and are available free of charge as a ".blq" file on the website [44], managed by the Onsala Space Observatory (OSO), Swedish national infrastructure for astronomy.

The best results can be obtained with the latest models, including: GOT4.7, FES2004, TPXO_Atlas, HAMTIDE, and DTU10, and it is also possible to view the models not available for specific areas on the OSO website (Figure 5).
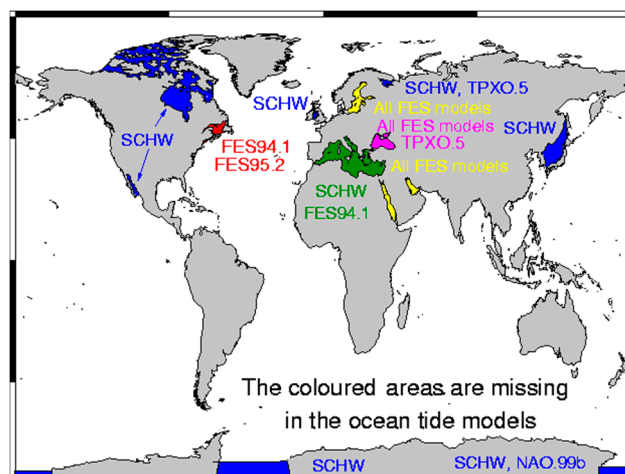

Figure 5. Map of areas where ocean tide patterns are missing, taken from [45].

Among the various available models, the GOT4.7 model is chosen, which is the latest version of Richard Ray's tide models and is one of the standard tide models, in addition to FES2004, used for satellite altitude corrections [46].

For the correction of the tropospheric delay, models commonly adopted for geodetic applications are used. These models are precise and complex [47], because they are based on satellite elevation angle and weather data, which cannot be easily determined. Based on literature considerations, in the current research a comparison between the Saastamoinen and Estimate ZTD (Zenith Total Delay) models is performed.

Finally, additional settings are set to obtain the desired PPP-static solution, including (Figure 6):

- Phwindup (phase wind-up), to correct the delay caused by the relative rotation between the satellite and receiver antennas;
- Reject Ecl, to exclude the GPS Block IIA satellites in eclipsed, that degrade the PPP solutions due to unpredicted behavior of yaw-attitude;
- RAIM (receiver autonomous integrity monitoring) FDE (fault detection and exclusion) to detect and exclude possible outliers from the measurements set used for the solution computation;
- Sat PCV e Rec PVC, to consider the phase center variations of the satellite and the receiver, respectively, feature allowed by uploading the "igs14.atx" file, provided by the IGS, containing the correction parameters of several types of antenna;
- a GDOP threshold is set to reject solution with GDOP value higher than 30, and a mask-angle equal to 10° is applied;
- no ambiguity resolution strategy is used;
- DCB multi-GNSS product, provided by the German aerospace center DLR, in ".bsz" format, is also used as an input (Figure 6).
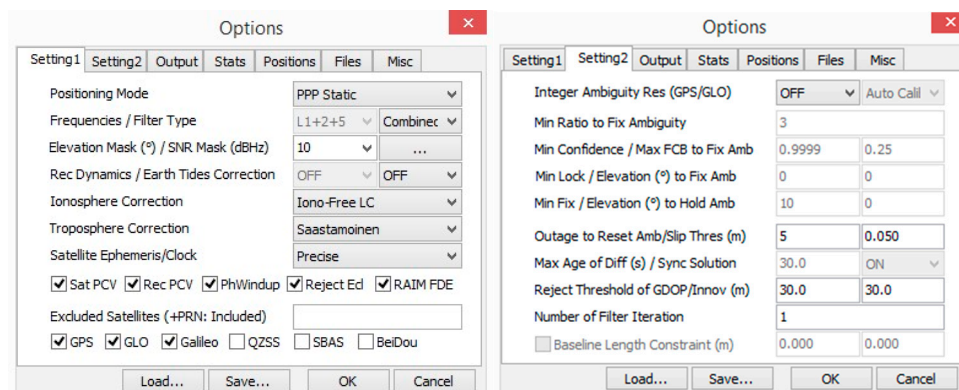
Figure 6. Output options interface with the RTKPOST module.

Defined by the described parameters, the aim of the paper is:

1. to verify and compare the impact of two tropospheric correction models (Saastamoinen and Estimate ZTD);
2. to evaluate the performance of PPP-static mode in terms of precision, accuracy and availability, using multi-GNSS data collected during two tests.

2.3. Comparison between Saastamoinen and Estimate ZTD Tropospheric Correction Models

As known by the literature, the atmosphere is the main error source for GNSS signals, and in particular two layers: the ionosphere and the troposphere. Ionospheric polarization can be mitigated using dual frequency receivers. Unlike ionospheric delay, the error caused by troposphere cannot be removed using the same procedure. The correction of tropospheric bias is often performed using a standard tropospheric model.

In RTKPOST, several tropospheric correction models can be applied, as described in Section 2.2. In order to verify the impact of different correction models on the positioning solution, two techniques are considered and their performances are compared: Saastamoinen and Estimate ZTD models.

The Saastamoinen model computes the tropospheric delay T_r using the following expression [48]:

$$T_r = \frac{0.002277}{\cos(z)}\left[p + \left(\frac{1255}{T} + 0.05\right)e - tan^2(z)\right]$$ (1)

where:

p, is the total pressure (hPa);
T, is the absolute temperature (K) of the air;
e, is the partial pressure (hPa) of water vapor;
z, is the zenith angle (rad).

In the Saastamoinen model [48], a standard atmosphere is considered as a reference, the geodetic height is approximated to the ellipsoidal height, and a humidity percentage is fixed to 70%.

The model considers the troposphere as divided into two layers. The first layer, from the earth surface to 10 km on it, has a constant descent rate of temperature of 6.5 C/km. The second layer, from 10 km to 70 km on the earth surface, has constant temperature value. Therefore, for atmospheric refraction integral, the function of refractive index can be computed based on the zenith distance trigonometric functions and term wise integration. In this way, the ZTD is expressed as:

$$ZTD = 0.002277 \frac{\left(P_0 + \left(0.05 + \frac{1255}{P_0 + 273.15}\right)e_0\right)}{f(\varphi, h)}$$ (2)

$$e_0 = rh \cdot 6.11 \cdot 10^{\frac{7.5T_0}{T_0 + 273.3}}$$ (3)

$$f(\varphi, h) = 1 - 0.00266cos2\varphi - 0.00028h$$ (4)

where P_0, T_0, and e_0 are, respectively, the surface pressure, the surface temperature, and the water vapor pressure at the surface level, rh is the relative humidity, $f(\varphi, h)$ is the correction of gravity acceleration caused by the rotation of the earth, and φ and h are the latitude and the height of point.

The Estimate ZTD model computes the tropospheric delay starting from the expression of the Saastamoinen model with the zenith angle and relative humidity equal to zero and employing the NMF (Niell Mapping Function), based on receiver geographical coordinates and measurement time [49]. The mapping function in terms of the elevation (El) and the azimuth (Az) angles between the satellite and the receiver is expressed as:

$$M(El) = M_w(E)\{1 + \cot(El) \cdot (G_N \cos(El) \cdot (G_N \cos(Az) + G_E \sin(Az))\}$$ (5)

$$T_{r,z} = M_h(El) \cdot Z_H + M(El)(Z_T - Z_H)$$ (6)

where Z_T (in m) is the tropospheric zenith total delay that is estimated from the Extended Kalman Filter together with the north (G_N) and the east (G_E) components of the tropospheric gradient. Z_H (in m) is the tropospheric zenith hydro-static delay computed using a tropospheric model, such as Saastamoinen, Hopfield, or modified Hopfield models with the zenith angle and relative humidity equal to zero. M_h (El) and M_w (El) are, respectively, the hydro-static and wet mapping-functions.

3. Results and Discussion

3.1. Preliminary Analyses (Test A)

In Test A, a permanent GNSS station stores measurements continuously for a month (July 2018), from triple constellations: GPS, GLONASS, and Galileo. In Table 1 and in Figure 7, the visibility during the data collection is resumed. In Table 1, the minimum, the maximum and the mean number of visible satellites are reported, for each considered GNSS combination. The GPS constellation provides the best coverage, with 5 minimum, 12 maximum, and 8 average number of visible satellites.

Fewer available satellites characterize GLONASS and Galileo; in fact, for both the mean number is 5. A significantly increased visibility is demonstrated by the double constellations, GPS+GLONASS, GPS+Galileo, GLONASS+Galileo; in particular, the GPS+GLONASS show the best visibility, with minimum, maximum, and mean number of visibility, respectively, 11, 12, and 15. In the triple GNSS configuration, GPS+GLONASS+Galileo, the visibility is further improved with a minimum of 14 available satellites, a maximum of 22, and a mean value of 17. The maximum number of visible satellites, for each day of the dataset and for each GNSS combination, is shown in Figure 7.

Table 1. Number of satellites.

GNSS Combination	Min	Mean	Max
GPS	5	8	12
GLONASS	4	5	7
Galileo	4	5	8
GPS+GLONASS	11	12	15
GPS+Galileo	9	12	15
GLONASS+Galileo	6	10	13
GPS+GLONASS+Galileo	14	17	22
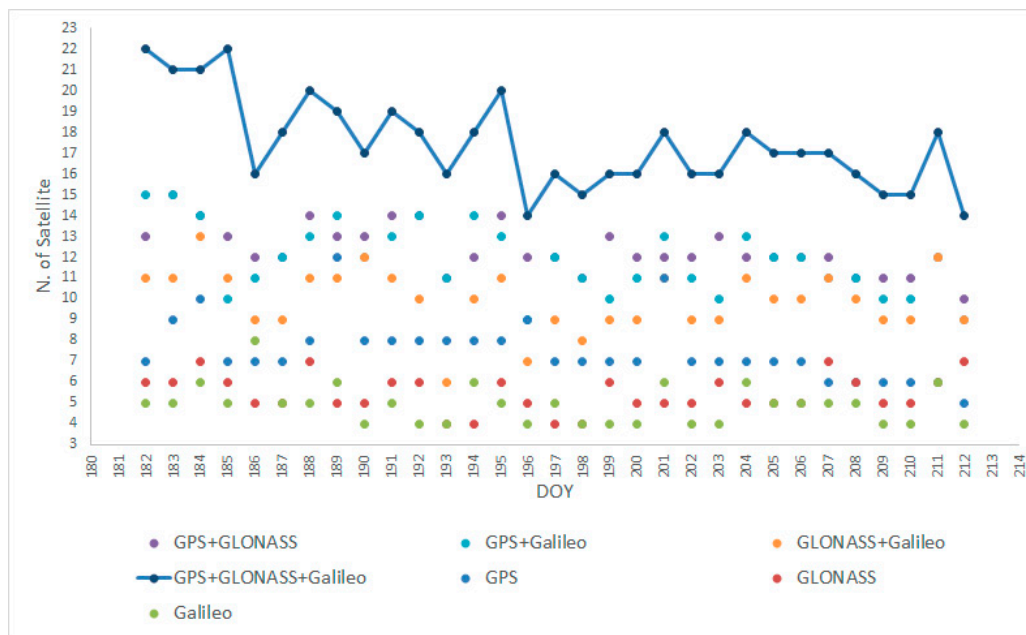
Figure 7. Number of maximum available satellites for each day of the dataset and for each Global Navigation Satellite System (GNSS) combination. DOY: Day of Year; GPS: Global Positioning System.

3.2. Performance of Multi-GNSS Static PPP Survey with Saastamoinen and Estimate ZTD Tropospheric Models (Test A)

In this section, the results of Test A are shown. In details, measurements from the considered GNSS combinations are processed in PPP mode, using the Saastamoinen and Estimate ZTD tropospheric models. The performance of the several configurations are compared in terms of precision and position error. Each of the 31 days is separately processed, obtaining the "daily solutions"; the "final solution" is the mean of the daily solutions and is compared with the known position of the station for error computation. The standard deviations of the daily solutions are also computed, in order to obtain information about the solution stability and precision.

In Table 2, the standard deviations σ of the considered configurations are shown. It is evident that the σ values are large, above all in the configurations including GPS, with both Saastamoinen and Estimate ZTD models.

Table 2. Standard deviation of the considered GNSS combinations with Saastamoinen and Estimate ZTD (Zenith Troposhperic Delay) tropospheric models.

GNSS Combination	Saastamoinen			Estimate ZTD		
	Standard Deviation (mm)			Standard Deviation (mm)		
	σ_x	σ_y	σ_z	σ_x	σ_y	σ_z
GPS	409	93	104	510	313	332
GLONASS	87	47	60	57	48	25
Galileo	101	69	67	292	54	462
GPS+GLONASS	125	17	73	84	17	54
GPS+Galileo	264	154	142	281	54	141
GLONASS+Galileo	77	35	59	54	42	36
GPS+GLONASS+Galileo	117	27	68	175	39	120

In Figure 8a, the X coordinates of the daily solutions, obtained processing GPS-only measurements with Estimate ZTD (black dots) and Saastamoinen (green dots) models, are represented. An anomalous solution, significantly different from the others, is evident at DOY 190, for both the tropospheric models. Further similar situations, relative to the other coordinates and to the other GNSS combinations, have been found. The RAIM-FDE algorithm of RTKLib did not detect outliers in measurements domain; nevertheless, the estimation process provides such anomalous solutions that could negatively affect the final solution. For this reason, an outlier rejection strategy in position domain is necessary too.

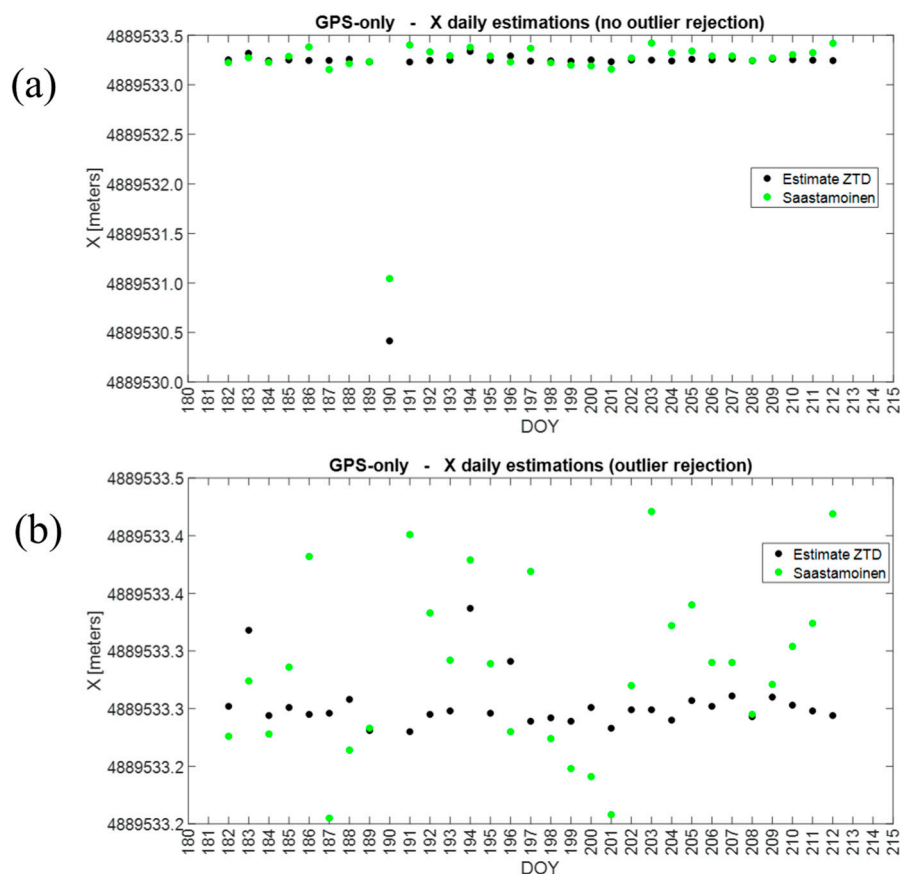**Figure 8.** Daily estimations of X component with Saastamoinen and Estimate ZTD (Zenith Troposhperic Delay) tropospheric models in case of GPS-only configuration (**a**) no outlier rejection (**b**) outlier rejection.

The outlier rejection strategy, adopted to improve the stability of the positioning, consists in discarding the daily solutions outsides the 6σ interval centered at the final solution [50,51]. The X

coordinates of the daily solutions for GPS-only case, after the rejection of the anomalous daily solutions, are shown in Figure 8b. The solutions in this case are clearly more consistent and the Estimate ZTD seems to provide more stable solutions with respect to the Saastamoinen model.

In Table 3, the standard deviations of the considered configurations, with the application of the previously mentioned outlier rejection strategy, are shown; in this case, the standard deviation values are significantly reduced with respect to the previous case (Table 2). Comparing the configurations with the Saastamoinen and Estimate ZTD tropospheric models, what becomes evident are the benefits of using the second one. Focusing on the configurations with Estimate ZTD model:

- the stabilities of single GNSS combinations are similar, with slightly best performance for GLONASS-only case;
- the stabilities of double GNSS combinations are increased with respect to the single GNSS case, the best performances are obtained with GPS+Galileo constellations, and the worst performances are obtained with GLONASS+Galileo;
- the stability of the triple GNSS combination is similar to double constellations cases.

Table 3. Standard deviation of the considered GNSS combinations with Saastamoinen and Estimate ZTD tropospheric models (outlier rejections).

GNSS Combination	Saastamoinen			Estimate ZTD		
	Standard Deviation (mm)			Standard Deviation (mm)		
	σ_x	σ_y	σ_z	σ_x	σ_y	σ_z
GPS	74	33	60	23	27	38
GLONASS	87	29	60	28	24	11
Galileo	101	51	67	30	29	16
GPS+GLONASS	69	17	55	25	10	10
GPS+Galileo	160	40	63	10	10	6
GLONASS+Galileo	77	28	59	33	26	23
GPS+GLONASS+Galileo	74	22	68	30	17	13

In Table 4, the position errors obtained with the considered configurations, applying the outlier rejection strategy, are shown. Even analyzing the position errors, it is evident the benefit of using Estimate ZTD with respect to the Saastamoinen model.

Table 4. Errors of the considered GNSS combinations with Saastamoinen and Estimate ZTD tropospheric models (outlier rejections).

GNSS Combination	Saastamoinen			Estimate ZTD		
	Error (mm)			Error (mm)		
	x	y	z	x	y	z
GPS	49	−3	37	17	3	18
GLONASS	26	−17	20	16	−4	10
Galileo	−64	−16	−43	−31	−5	−29
GPS+GLONASS	36	−8	28	11	1	10
GPS+Galileo	−6	14	11	−2	8	−2
GLONASS+Galileo	1	−19	−4	−5	−8	−6
GPS+GLONASS+Galileo	21	5	11	1	−2	2

Focusing only on configurations with the Estimate ZTD model, the GPS-only and GLONASS-only performances are very similar, while larger errors are evident for the Galileo-only case. The use of double constellations is surely advantageous and, in particular, a sub-cm level positioning is obtained with the GPS+Galileo combination. The better stability of GPS and Galileo, with respect to GLONASS,

is analyzed by other authors [10,11,52]. Indeed, the GLONASS system adopts FDMA (Frequency Division Multiple Access) techniques while, conversely, GPS and Galileo use CDMA (Code Division Multiple Access) techniques, fulfilling the signal-in-space interoperability requirement (identical center frequencies of interoperable signals). Thus, GLONASS is not "signal interoperable" with GPS or Galileo, but it is "system interoperable" (referring to the ability of GNSSs to be used together to provide better capabilities at the user level than would be reached by using a single system) [52]. In more detail, using FDMA signals, different hardware delay biases exist in the GLONASS receiving channel (also referred to as inter-frequency or inter-channel biases). In [10], the authors noticed that integrating a few GLONASS satellites (as in the current research the mean GLONASS satellites mean number is equal to 5) will not contribute to the positioning accuracy when there is a sufficient number of GPS satellites. The same authors analyzed the residuals for the IF code and phase observations from combined GPS/GLONASS PPP and the results related to GLONASS code residuals were significantly larger than the GPS one, while carrier phase residuals were very close for GPS and GLONASS. For the authors in [10], the obtained results are related to the larger GLONASS satellite clock and orbit residuals errors and to the neglected code hardware delay biases. Conversely, in [11] the RMS values of GLONASS code residuals were slightly lower than GPS. This different conclusion from [10] is related to the fact that the GLONASS inter-frequency biases were well threated in their customized multi-GNSS positioning model developed and proposed in [11].

Finally, in Table 4 an error of few mm is obtained with the triple constellation GPS+GLONASS+Galileo.

3.3. Performance of Multi-GNSS Static PPP Survey with CNES/CLS (Test A)

The measurements of Test A are processed with the PPP technique. In order to maintain the data consistency, precise orbits and clock products from CNES/CLS are adopted; clock data with a sampling of 30 s are used.

In Table 5, the results obtained processing GPS-only measurements with the PPP technique are shown. The results are expressed in terms of daily solution standard deviations and final solution errors. In order to assess the effect of the usage of precise clock data at 30 s (second line of Table 5), a comparison is carried out with the performance of standard GPS-PPP using clock data at 15 min (first line of Table 5). For all the considered configurations, the Estimate ZTD tropospheric model and the previously mentioned outlier rejection strategy are used.

Table 5. Standard deviations and errors of GPS-PPP (Precise Point Positioning) with 15 min clock data and GPS-PPP with 30 s clock data. Estimate ZTD tropospheric model and outlier rejection strategy are used.

GNSS	Data	Technique	Standard Deviation (mm)			Error (mm)		
			σ_x	σ_y	σ_z	x	y	z
GPS	Clock 15 min	PPP	23	27	38	17	3	18
GPS	Clock 30 s	PPP	6	5	4	−13	2	−3

Comparing the lines 1 and 2 of Table 5, it is evident that using precise clock products at 30 s provides significant benefits in terms of both standard deviation and error; indeed, all the considered figures of merit are reduced by one order of magnitude.

3.4. Performance of Multi-GNSS Static PPP Survey (Test B)

In this section, the results obtained processing the measurements of Test B, with the standard PPP algorithm, are shown. All possible combinations of GPS, GLONASS, and Galileo are considered, the Estimate ZTD tropospheric model is adopted, and the outlier rejection strategy is applied (Table 6).

Table 6. Standard deviations and errors of the considered GNSS combinations with Estimate ZTD tropospheric models (outlier rejections).

GNSS Combination	Standard Deviation (mm)			Error (mm)		
	σ_x	σ_y	σ_z	x	y	z
GPS	77	144	23	−53	−171	−27
GLONASS	26	83	16	−9	91	20
Galileo	744	568	466	218	188	27
GPS+GLONASS	40	57	13	−55	−31	−4
GPS+Galileo	63	109	13	−47	−149	−24
GLONASS+Galileo	74	66	79	−4	75	9
GPS+GLONASS+Galileo	31	50	9	−49	−1	−1

For Test B, all the considered configurations demonstrate worse performance with respect to homologous configurations in Test A; this is probably related to the different equipment adopted in the two tests and, above all, to different amounts of processed data, significantly larger in Test A.

About the single GNSS configurations, the GLONASS-only case provides the best results in terms of both standard deviation and error, while degraded performances are evident for the GPS-only and, above all, for the Galileo-only case. The double constellations cases demonstrate better performance with respect to single constellation ones; the best performance between the double constellation configurations is GPS+GLONASS with a tridimensional error of about 6 cm.

Triple constellation GPS+GLONASS+Galileo has the best performance according to all the figures of merit; in particular, in this case the tridimensional standard deviation and error are, respectively, about 6 cm and 5 cm.

4. Conclusions

In this work, the performances of static multi-GNSS PPP are analyzed; several configurations are considered. The used GNSS are GPS, GLONASS, and Galileo and all their possible combinations are assessed. Two different tropospheric models are tested: Saastamoinen and Estimate ZTD. The benefit of using precise clock products at 30 s, instead of classic products at 15 min, is evaluated.

In order to carry out a significant analysis, a large amount of data is processed

- A dataset of GNSS measurements, stored at a permanent station, acquiring 24 h a day for 1 month (Test A)
- A dataset of GNSS measurements, stored by a geodetic receiver on a pillar, acquiring about 6 h a day for 10 days (Test B)

The open-source software RTKLib is used for the processing. Daily solutions are obtained by RTKLib, their standard deviation is considered to assess the stability of the processing, while the mean of the daily solutions is the final solution. The known position of the used receivers is the reference for the error analysis.

Final solutions and standard deviations of the daily solutions are used to implement an outlier rejection strategy in the position domain due to the inefficiency of the applied RAIM-FDE algorithm to detect and exclude the outlier from the measurements set.

From the comparison between the tropospheric models Saastamoinen and Estimate ZTD, it is clear that the second allows for better performance. About the GNSS combinations, GPS-only and GLONASS-only cases provided similar performance, while the Galileo-only performances are slightly degraded. The use of double constellations is generally beneficial, and particularly promising results are obtained with the GPS+Galileo combination. The triple combination GPS+GLONASS+Galileo provides the best performance for both tests; in particular, errors of a few millimeters are obtained in Test A, and one order of magnitude larger for Test B, probably because the last is significantly shorter.

The use of precise clock products at 30 s demonstrates to increase significantly the PPP performance; indeed, in GPS-only case the tridimensional error from 2.5 cm (with the clock data at 15 min) to 1.3 cm (with the clock data at 30 s).

Conflicts of Interest: The authors declare no conflict of interest.

References

1. Gao, Y.; Wang, M. Precise point positioning for deformation monitoring using post-mission and real-time precise orbit and clock products. *Geophys. Res. Abstr.* **2007**, *9*, 03155.
2. Wang, G.Q. Millimeter-accuracy GPS landslide monitoring using Precise Point Positioning with Single Receiver Phase Ambiguity (PPP-SRPA) resolution: A case study in Puerto Rico. *J. Geod. Sci.* **2013**, *3*, 22–31. [CrossRef]
3. Capilla, R.M.; Berné, J.L.; Martín, A.; Rodrigo, R. Simulation case study of deformations and landslides using real-time GNSS precise point positioning technique. *Geomat. Nat. Hazards Risk* **2016**, *7*, 1–18. [CrossRef]
4. Bisnath, S.; Gao, Y. Current State of Precise Point Positioning and Future Prospects and Limitations. *Int. Assoc. Geod. Symp.* **2009**, *133*, 615–623.
5. Geng, J.; Teferle, F.N.; Meng, X.; Dodson, A.H. Kinematic precise point positioning at remote marine platforms. *GPS Solut.* **2010**, *14*, 343–350. [CrossRef]
6. Tegedor, J.; Øvstedal, O.; Vigen, E. Precise orbit determination and point positioning using GPS, GLONASS, Galileo and BeiDou. *J. Geod. Sci.* **2014**, *4*, 65–73. [CrossRef]
7. Innac, A.; Angrisano, A.; Gaglione, S.; Crocetto, N. GPS precise positioning techniques for remote marine applications. In Proceedings of the 2019 IMEKO TC19 International Workshop on Metrology for the Sea, Genova, Italy, 3–5 October 2019; IMEKO-International Measurement Federation Secretariat: Budapest, Hungary, 2020; pp. 81–85.
8. Melgard, T.; Vigen, E.; De Jong, K.; Lapucha, D.; Visser, H.; Ørpen, O. G2—The first real-time GPS and GLONASS Precise orbit and clock service. In Proceedings of the 22nd International Technical Meeting of the Satellite Division of the ION, Savannah, GA, USA, September 22–25 2009; pp. 1885–1891.
9. Cai, C.; Gao, Y. Precise point positioning using combined GPS and GLONASS observations. *J. Glob. Position. Syst.* **2007**, *6*, 13–22. [CrossRef]
10. Cai, C.; Gao, Y. Modeling and assessment of combined GPS/GLONASS precise point positioning. *GPS Solut.* **2013**, *17*, 223–236. [CrossRef]
11. Li, X.; Zhang, X.; Ren, X.; Fritsche, M.; Wickert, J.; Schuh, H. Precise positioning with current multi-constellation Global Navigation Satellite System: GPS, GLONASS, Galileo and BeiDou. *Sci. Rep.* **2014**, *5*, 8328. [CrossRef]
12. Afifi, A.; El-Rabbany, A. An innovative dual frequency PPP model for combined GPS/Galileo observations. *J. Appl. Geod.* **2015**, *9*, 27–34. [CrossRef]
13. Afifi, A.; El-Rabbany, A. Precise Point Positioning Using Triple GNSS Constellations in Various Modes. *J. Appl. Geod.* **2016**, *10*, 779. [CrossRef] [PubMed]
14. Guo, F.; Li, X.; Zhang, X.; Wang, J. The contribution of Multi-GNSS Experiment (MGEX) to precise point positioning. *Adv. Space Res.* **2015**, *59*, 2714–2725. [CrossRef]
15. Zhang, X.; Liu, J.; Forsberg, R. Application of precise point positioning in airborne survey. *Geomat. Inf. Sci. Wuhan Univ.* **2006**, *31*, 19–22. (In Chinese)
16. Cai, C.; Gao, Y.; Pan, L.; Zhu, J. Precise point positioning with quad-constellations: GPS, Beidou, GLONASS and Galileo. *Adv. Space Res.* **2015**, *56*, 133–143. [CrossRef]
17. Pandey, D.; Dwivedi, R.; Dikshit, O.; Singh, A.K. GPS and glonass combined static precise point positioning (PPP). *Int. Arch. Photogramm. Remote Sens. Spat. Inf. Sci.* **2016**, *41*, 483–488. [CrossRef]

18. Angrisano, A.; Gaglione, S.; Gioia, C. Performance assessment of GPS/GLONASS single point positioning in an urban environment. *Acta Geod. Geophys.* **2013**, *48*, 149–161. [CrossRef]

19. Guo, J.; Li, X.; Chen, X.; Geng, J.; Wen, Q.; Pan, Y. Performance Analysis of Multi-GNSS Precise Point Positioning. In *China Satellite Navigation Conference*; Springer: Singapore, 2017.

20. Abd Rabbou, M.; El-Rabbany, A. Performance analysis of precise point positioning using multi-constellation GNSS: GPS, GLONASS, Galileo and BeiDou. *Surv. Rev.* **2017**, *49*, 39–50. [CrossRef]

21. El Manaily, E.; Adb Rabbou, M.; El-Shazly, A.; Baraka, M. Evaluation of quad-constellation GNSS precise point positioning in Egypt. *Artif. Satel.* **2017**, *52*, 9–18. [CrossRef]

22. Pan, L.; Zhang, X.; Li, X.; Li, X.; Lu, C.J.; Liu, J.; Wang, Q. Satellite availability and point positioning accuracy evalutation on a global scale for integration of GPS, GLONASS, BeiDou and Galileo. *Adv. Space Res.* **2019**, *63*, 2696–2710. [CrossRef]

23. Van Bree, R.J.P.; Tiberius, C.C.J.M. Real-time single-frequency precise point positioning: Accuracy assessment. *GPS Solut.* **2012**, *16*, 259–266. [CrossRef]

24. Innac, A.; Gaglione, S.; Angrisano, A. Multi-GNSS Single Frequency Precise Point Positioning. In Proceedings of the 2018 IEEE International Workshop on Metrology for the Sea; Learning to Measure Sea Health Parameters (MetroSea), Bari, Italy, 8–10 October 2018.

25. Innac, A.; Angrisano, A.; Gaglione, S.; Vultaggio, M.; Crocetto, N. Performance Comparison among Multi-GNSS Single Frequency Precise Point Positioning Techniques. *Kartografija i geoinformacije (Cartogr. Geoinf.)* **2019**, *18*, 80–99. [CrossRef]

26. Zrinjski, M.; Barković, Đ.; Matika, K. Development and modernization of GNSS [Razvoj i modernizacija GNSS-a]. *Geod. List* **2019**, *73*, 45–65.

27. Abd Rabbou, A.M.; El-Shazly, A.; Ahmed, K. Comparative analysis of multi-constellation GNSS single-frequency precise point positioning. *Surv. Rev.* **2017**, *50*, 373–382. [CrossRef]

28. Dardanelli, G.; Lo Brutto, M.; Pipitone, C. GNSS CORS Network of the University of Palermo: Design and first analysis of data. *Geogr. Tech.* **2020**, *15*, 43–69. [CrossRef]

29. Dardanelli, G.; Carella, M. Integrated surveying with mobile mapping system, EGNOS, NRTK and laser technologies in the park "Ninni Cassarà" in Palermo. *ISPRS Ann. Photogramm. Remote Sens. Spat. Inf. Sci.* **2013**, *2*, 95–100. [CrossRef]

30. Dardanelli, G.; Paliaga, S.; Allegra, M.; Carella, M.; Giammarresi, V. Geomatic applications to urban park in Palermo. *Geogr. Tech.* **2015**, *10*, 28–43.

31. Dardanelli, G.; La Loggia, G.; Perfetti, N.; Capodici, F.; Puccio, L.; Maltese, A. Monitoring displacements of an earthen dam using GNSS and remote sensing. *Proc. SPIE Int. Soc. Opt. Eng.* **2014**, *9239*, 923928.

32. Dardanelli, G.; Pipitone, C. Hydraulic models and finite elements for monitoring of an earth dam, by using GNSS techniques. *Period. Polytech. Civ. Eng.* **2017**, *61*, 421–433. [CrossRef]

33. Pipitone, C.; Maltese, A.; Dardanelli, G.; Brutto, M.L.; La Loggia, G. Monitoring water surface and level of a reservoir using different remote sensing approaches and comparison with dam displacements evaluated via GNSS. *Remote Sens.* **2018**, *10*, 71. [CrossRef]

34. Stocchi, P.; Antonioli, F.; Montagna, P.; Pepe, F.; Lo Presti, V.; Caruso, A.; Corradino, M.; Dardanelli, G.; Renda, P.; Frank, N.; et al. A stalactite record of four relative sea-level highstands during the Middle Pleistocene Transition. *Quat. Sci. Rev.* **2017**, *173*, 92–100. [CrossRef]

35. Lo Brutto, M.; Dardanelli, G. Vision metrology and Structure from Motion for archaeological heritage 3D reconstruction: A Case Study of various Roman mosaics. *Acta IMEKO* **2017**, *6*, 35–44. [CrossRef]

36. Ebolese, D.; Lo Brutto, M.; Dardanelli, G. Uav survey for the archaeological map of lilybaeum (Marsala, Italy). *ISPRS Ann. Photogramm. Remote Sens. Spat. Inf. Sci.* **2019**, *42*, 495–502. [CrossRef]

37. Barreca, G.; Bruno, V.; Dardanelli, G.; Guglielmino, F.; Lo Brutto, M.; Mattia, M.; Pipitone, C.; Rossi, M. An integrated geodetic and InSAR technique for the monitoring and detection of active faulting in southwestern Sicily. *Ann. Geophys.* **2020**, *63*, EP03. [CrossRef]

38. Dawidowicz, K.; Krzan, G. Periodic signals in a pseudo-kinematic GPS coordinate time series depending on the antenna phase centre model–TRM55971.00 TZGD antenna case study. *Surv. Rev.* **2017**, *49*, 268–276. [CrossRef]

39. Bilich, A.; Mader, G.L. GNSS absolute antenna calibration at the National Geodetic Survey. In Proceedings of the 23rd International Technical Meeting of the Satellite Division ofThe Institute of Navigation, Portland, OR, USA, 21–24 September 2010; Volume 2, pp. 1369–1377.

40. Takasu, T.; Kubo, N.; Yasuda, A. Development, Evaluation and Application of RTKLIB: A program library for RTK-GPS. In Proceedings of the GPS/GNSS Symposium, Tokyo, Japan, 20 August 2007.

41. Rizos, C.; Janssen, V.; Roberts, C.; Grinter, T. Precise Point Positioning: Is the Era of Differential GNSS Positioning Drawing to an End? (2012). Available online: http://eprints.utas.edu.au/13280/1/2012_Rizos_etal_FIG-WW-2012_proceedings_version.pdf (accessed on 26 June 2020).

42. Seepersad, G.; Bisnath, S. Challenges in Assessing PPP Performance. *J. Appl. Geod.* **2014**, *8*, 205–222. [CrossRef]

43. IGS International GNSS Service. Available online: http://mgex.igs.org/IGS_MGEX_Products.php (accessed on 26 June 2020).

44. Free ocean tide loading provider. Available online: http://holt.oso.chalmers.se/loading/ (accessed on 26 June 2020).

45. Free ocean tide loading provider. Available online: http://holt.oso.chalmers.se/loading/tidemodels.html (accessed on 26 June 2020).

46. Zawadzki, L.; Ablain, M.; Carrere, L.; Ray, R.D.; Zelensky, N.P.; Lyard, F.; Guillot, A.; Picot, N. Investigating the 59-Day Error Signal in the Mean Sea Level Derived from TOPEX/Poseidon, Jason-1, and Jason-2 Data with FES and GOT Ocean Tide Models. *IEEE Trans. Geosci. Remote Sens.* **2018**, *56*, 3244–3255. [CrossRef]

47. Xu, G. *GPS: Theory, Algorithms, and Applications*; Springer: Berlin/Heidelberg, Germany, 2007.

48. Saastamoinen, J. Atmospheric correction for troposphere and stratosphere in radio ranging of satellites. In *The Use of Artificial Satellites for Geodesy*; Henriksen, S.W., Mancini, A., Chovitz, B.H., Eds.; AGU: Washington, WA, USA, 1972; Volume 15, pp. 247–252.

49. Niell, A.E. Global mapping functions for the atmosphere delay at radio wavelengths. *J. Geophys. Res.* **1996**, *101*, 3227–3246. [CrossRef]

50. Barbarella, M.; Gandolfi, S.; Tavasci, L. Monitoring of the Italian GNSS geodetic reference frame. In *New Advanced GNSS and 3D Spatial Techniques*; Springer: Cham, Switzerland, 2018; pp. 59–71.

51. Gandolfi, S.; Tavasci, L.; Poluzzi, L. Improved PPP performance in regional networks. *GPS Solut.* **2016**, *20*, 485–497. [CrossRef]

52. Hein, G. GNSS interoperability: Achieving a global system of systems or does everything have to be the same. *Inside GNSS* **2006**, *1*, 57–60.